Intraoperative Direct Subcortical Stimulation: Comparison of Monopolar and Bipolar Stimulation

Jose Gomez-Tames[a], Takaharu Kutsuna[a], Manabu Tamura[b,c], Yoshihiro Muragaki[b,c], Akimasa Hirata[a]

a. Nagoya Institute of Technology, Department of Electrical and Mechanical Engineering, Nagoya, Aichi 466-8555, Japan

b. Faculty of Advanced Techno-Surgery, Institute of Advanced Biomedical Engineering and Science, Tokyo Women's Medical University, Shinjuku-ku, Tokyo 162-8666, Japan

c. Department of Neurosurgery, Neurological Institute, Tokyo Women's Medical University, Shinjuku-ku, Tokyo 162-8666, Japan

*Corresponding Author: Jose Gomez-Tames

Tel & Fax: +81-52-735-7916

E-mail:jgomez@nitech.ac.jp

This is an author-created, un-copyedited version of an article published in Physics in Medicine and Biology. IOP Publishing Ltd is not responsible for any errors or omissions in this version of the manuscript or any version derived from it. The Version of Record is available online at https://doi.org/10.1088/1361-6560/aaea06

Abstract

Intraoperative subcortical electrical stimulation is used to identify and preserve white matter tracts so that tumor resection can be performed while avoiding postsurgical deficits. The effects of the stimulating electrodes in identifying the white matter tracts have not been characterized; thus, different hospitals use different electrode configurations. Computational modeling can be used to conduct a systematic assessment of the effects of the stimulating electrode parameters. However, no realistic computational model of subcortical electrical stimulation has been implemented and verified. In this study, we investigated the interaction between the corticospinal tract (CST) and subcortical stimulation and compared different electrode configurations during monopolar and bipolar stimulation. For that, we computed the induced electric field in a realistic human head model coupled with a CST axon model. The implemented model was verified with available experimental data that were acquired during subcortical stimulation, and a systematic sensitivity analysis of parameters related to the stimulation was conducted. The results showed that the optimal stimulation varies according to the surgery conditions. If the CST was close to the resection border, bipolar stimulation could produce more selective activation. Monopolar stimulation was more robust and more effective for the CST far from the stimulation point.

Keywords: Subcortical Stimulation; Brain Surgery; Monopolar Electrode; Bipolar Electrode

1. Introduction

Maximal resection of intracranial gliomas improves prognosis, but may be associated with neurological deterioration due to the risk of a lesion of white matter tracts in or near motor-eloquent regions, such as the corticospinal tract (CST) (Saito et al. 2015; Saito et al. 2014; Smith et al. 2008; Hervey-Jumper et al. 2015). To reduce the risk of a lesion, intraoperative direct subcortical electrical stimulation ("subcortical stimulation") is applied at the resection cavity for identification and integrity assessment of white matter tracts (Kamada et al. 2009; Fukaya et al. 2011; Prabhu et al. 2011; Yamaguchi et al. 2007; Shiban et al. 2015; Mikuni et al. 2007; Enatsu et al. 2016).

For subcortical stimulation, monopolar (Kamada et al. 2009; Saito et al. 2014; Fukaya et al. 2011; Raabe et al. 2014) or bipolar (Yamaguchi et al. 2007; Mikuni et al. 2007; Duffau et al. 2002) probe tips ("electrodes") are used by different groups; the stimulating electrode geometry is also different. In monopolar stimulation, the cathodic electrode is placed on the resection border and the reference electrode on the shoulder or forehead, while bipolar stimulation uses two adjacent electrodes, both of which are in contact with the brain. The appropriate electrode depends on the clinical context and may change within the same surgery according to ongoing modifications during the procedure (Bello et al. 2014). However, the selection of the stimulation parameters is based on personal experience or conventional usage owing to the lack of a systematic assessment of the effects of the stimulation parameters (Szelényi et al. 2011; Bello et al. 2014; Fukaya et al. 2011).

Systematic assessment of stimulation parameters can be performed using computational simulations, such as orientation, location, and design of coils for transcranial magnetic stimulation (Nummenmaa et al. 2014; Janssen et al. 2014; Laakso et al. 2014; Iwahashi et al. 2017; Deng et al. 2013; Gomez-Tames, Hamasaka, et al. 2018). Also, computational models have been applied for cortical stimulation (Manola et al. 2005; Seo et al. 2015; Gomez-Tames, Akimasa, et al. 2018; Seo et al. 2017). However, similar techniques have not been applied to

subcortical stimulation except for (Mandonnet & Pantz 2011), in which the effect of bipolar electrode orientation was investigated in a simplified geometrical model.

In this study, a computational model was implemented to investigate the interaction between the CST and subcortical stimulation to compare different electrode configurations during monopolar and bipolar stimulation, with the final aim of identifying the most effective stimulation parameters used in clinical practice. The computational model is a two-step calculation: (1) the electric field produced in a realistic head model by the injected current through the electrodes and (2) the elicited action potentials of CST axons. For the first time, the proposed model was verified using the threshold–distance relationship measured in subcortical stimulation.

2. Materials and methods

2.1 Head Model

A human-head model with a resolution of 0.5 mm was employed (Laakso et al. 2015), as shown in Figure 1A. This model was constructed from T1- and T2-weighted magnetic resonance images acquired using a 3T magnetic resonance imaging scanner and represented in the form of a grid of cubical voxels (65.3×10^6 voxels). The model was segmented into a total of 14 tissues and body fluids (skin, fat, muscle, cortical bone, marrow bone, gray matter, white matter, cerebellar gray matter, cerebellar white matter, brainstem, nuclei, ventricles, cerebrospinal fluid (CSF), and eye tissues) using in-house software (Laakso et al. 2015) equipped with the FreeSurfer brain imaging software package (Dale et al. 1999). To simulate subcortical stimulation in a craniotomy, brain tissue was removed from the original head model (see Figure 1A). The moisture conditions during resection were considered by adding a layer of 0.5 mm with the same conductivity as that of CSF on the resection border.

2.2 Volume Conductor Model

The electric potential generated by the electrodes attached to the resection border was computed using the scalar potential finite-difference method with successive-over-relaxation and multigrid methods (Dawson & Stuchly 1998; Laakso & Hirata 2012) to solve the scalar potential equation

$$\nabla \cdot (\sigma \nabla \mathrm{V}_e) = 0, \tag{1}$$

where V_e and σ denote the scalar potential and tissue conductivity, respectively. There were 6 multigrid levels was six (Laakso & Hirata 2012), and the iteration continued until the relative residual was less than 1×10^{-6}; for this residual, the error relative to the maximum voxel internal electric field was less than 0.5%. The tissue conductivities were determined using the fourth-order Cole–Cole model at 5 kHz (S. Gabriel et al. 1996). Illustrative computation results are presented in Figure 1B and Figure 1C for monopolar and bipolar stimulation, respectively.

2.3 Subcortical Axon Model

The effects of the extracellular electric field on nerve axons was described by the following general equation (McNeal 1976; Rattay 1999):

$$c_m \frac{dV_{m,n}}{dt} + \sum_x g_x (V_m - V_x) - \frac{\Delta^2 V_{m,n}}{R} = \frac{\Delta^2 V_e}{R} \tag{2}$$

where c_m is the membrane capacitance, and $V_\mathrm{m,n}$ is the membrane potential at position n along the nerve axon that corresponds to $V_\mathrm{e,n} - V_\mathrm{i,n}$ (refer to the equivalent circuit of the axon in Figure 2). The axons of a myelinated nerve consist of internodes (segments ensheathed by myelin) and nodes of Ranvier (ionic channels) that are modeled by the conductance term g_x and reversal potential V_x, as shown in Figure 2A. At the nodes of Ranvier, the ionic membrane current was formulated as a conductance-based voltage-gated model. In this study, the Chiu–Ritchie–Rogart–Stagg–Sweeney model was considered (Sweeney et al. 1987). At the myelinated internodes, the leak conductance was modeled as a passive element.)

The right-hand side of Equation 2 includes $\Delta^2 V_e = V_{e,n-1} - 2V_{e,n} + -2V_{e,n+1}$, which describes the driving term resulting from the extracellular electrical potential. The variable *R* denotes the intra-axonal resistance between the centers of two adjacent compartments. The activation threshold (i.e., the lowest stimulation intensity necessary to propagate an action potential in a given axon) was obtained using the bisection search method until the error was lower than 10 μA. An action potential was considered to have been elicited when the transmembrane potential exceeded a depolarization of 80 mV in at least 4 successive nodes and at successive times (Gomez-Tames et al. 2012; Gomez-Tames et al. 2013). The nerve axon diameter was 13 μm within the Betz cell's axon diameter range (Rivara et al. 2003; Firmin et al. 2014; Guyton & Hall 2006).

2.4 Stimulation Parameters

Monopolar and bipolar electrodes were investigated based on the geometries used in clinical practice. The diameter of the electrode was 1–3 mm for monopolar or bipolar stimulation (Yamaguchi et al. 2007; Mikuni et al. 2007; Duffau et al. 2002; Szelényi et al. 2010; Fukaya et al. 2011; Bello et al. 2014; Raabe et al. 2014; Kamada et al. 2009). The inter-electrode distance was 3–10 mm in the case of bipolar stimulation (Yamaguchi et al. 2007; Mikuni et al. 2007; Duffau et al. 2002; Szelényi et al. 2010). The most common geometries in clinical practice are summarized in Table 1. In the monopolar stimulation, the distant anode (reference electrode) was placed on the lateral side of the neck below the ear (left or right) or forehead (Fukaya et al. 2011; Bello et al. 2014; Szelényi et al. 2011), as shown in Figure 1A. Because the typical maximum current is 15 mA in subcortical stimulation (Fukaya et al. 2011; Bello et al. 2014; Szelényi et al. 2011; Riva et al. 2016; Kamada et al. 2009), the intensity varied between 1 mA and 15 mA. The stimulation waveform was a monophasic pulse of 0.2-ms duration (Kamada et al. 2009).

2.5 Activation Map and Indexes

Descending subcortical axons were placed in a grid of 15×25 mm^2 close to the stimulation site in the white matter, as shown in Figure 2A. The minimum injection current was obtained to activate the subcortical axon model at each position of the grid. The resulting activation map can be observed in Figure 2B. Stimulation area and depth were used as indices to compare the effect on the maps of the different electrode configurations (Table 1). Stimulation depth is used in clinical practice as a metric to evaluate when to stop resection to avoid extraction of non-affected brain regions (Kamada et al. 2009; Fukaya et al. 2011; Prabhu et al. 2011; Yamaguchi et al. 2007; Shiban et al. 2015; Mikuni et al. 2007; Enatsu et al. 2016). Stimulation area is used to quantify the dispersion of the stimulation. Stimulation depth was determined as the deepest position that an axon can be activated in the activation map grid for a specific injection current intensity. Similarly, the stimulation area was the area in which the axons in the activation map grid were activated for a specific injection current intensity. In addition, selectivity was considered as the stimulation depth divided by the stimulation area. For instance, a higher stimulation depth with smaller stimulation area represented a focal stimulation.

2.6 Assumption Analysis

Three assumptions were considered in subsections 3.1 and 3.2: no tumor was remaining following resection when subcortical stimulation was applied, axons descended straight in the superior–inferior direction, and moisture was controlled during the surgery.

The validity of these assumptions was examined in subsection 3.3 by considering the following model modifications. (A) A tumor layer replaced the white matter tissue next to the resection border wall. Its length was the same as that of the resection border wall, and its thickness was 1–5 mm (Figure 6). The tumor conductivity (σ_{tumor}) was set to 0.2 S/m or 0.5 S/m (Latikka et al. 2001; Aonuma et al. 2018). Note that an exact tumor conductivity value is difficult to determine owing to cancerization degree, but it is consistently larger than that of the surrounding tissues

(white and gray matter) (Song et al. 2016; Lu et al. 1992; Voigt et al. 2011). (B) The inclination of the axon's trajectory was considered by rotating the axon between -15° to 15° about its media-lateral axis (Christidi et al. 2016). (C) Moisture thicknesses of 0.25, 0.5, and 1 mm were examined. The model resolution of 0.25 mm was used only for the computation of the thinnest moisture thickness. Variation in the resolution had a marginal effect in the voltage distribution (less than 2% of the mean error in the vicinity of the resection border).

To quantify the effect of the assumptions, we calculated the relative error of the injection current to achieve different stimulation depths (1–5 mm) and areas (10–50 mm^2) between (A-C) models and the reference activation map, as shown in Figure 6D (electrode diameter of 3 mm and an inter-electrode distance of 5 mm).

3. Results

First, threshold distance measurements during subcortical stimulation were used to verify the implemented model. Second, computed activation maps were used to investigate the impact of the electrode parameters (diameter and inter-electrode distance) on the stimulation region. Finally, we quantified the effects of different model assumptions (tumor conductivity and thickness, axon inclination, and moisture of resection border) on the stimulation region.

3.1 Subcortical Stimulation Model Verification

The implemented model was verified with the threshold–distance relationship measured in (Kamada et al. 2009). In their study, the best stimulus point (minimum stimulation intensity) was found on the resection border to activate the motor-eloquent region in 18 patients. Second, the minimum distance between the best stimulus point and CST was obtained in each patient (offline measurement). In our model, the distance between the resection border and axon was considered between 1 and 15 mm (the axon was fixed while the resection border was modified). Similar to that in the experiment, a monopolar cathode 3 mm in diameter was used with a pulse duration of 0.2 ms.

Simulation and experimental threshold–distance relationships are presented in Figure 3. Considering the uncertainty of the CST axon diameters (10 to 15 μm in the literature (Rivara et al. 2003; Firmin et al. 2014; Guyton & Hall 2006)), the simulation results were within the measurements' variability. The best-fitting curve was obtained using an axon diameter of 13 μm ($R^2 = 0.999$, $p < 0.001$, and root mean square error of 0.71 mA).

3.2 Electrode Parameters Effect

The activation maps show the effects of monopolar and bipolar stimulations using the conditions in Table 1, as shown in Figure 4A and Figure 4B. In monopolar stimulation, the activation maps were almost identical, regardless of the location of the distant anode and electrode diameter. In bipolar stimulation, the stronger activation (i.e., deeper and broader area) occurred under the cathode. In general, large inter-electrode distances and small diameters presented strong activation in bipolar stimulation at the same injection current. In particular, a 10-mm inter-electrode distance presented an activation stronger than that of 5 mm at the same electrode diameter. Similarly, a 5-mm inter-electrode distance had a stronger activation than that of 3 mm for the same electrode diameter. For smaller current intensities, a 1-mm electrode diameter also showed a stronger activation than that of 3 mm at the same inter-electrode distance.

The relationship between activation area and depth is presented in Figure 5-A1 and Figure 5-A2 for monopolar ($R^2 = 0.997$) and bipolar ($R^2 = 0.9789$) stimulation, respectively. Figure 5-A2 also describes how selectivity varied between both electrode configurations. Bipolar stimulation had a deeper activation than monopolar stimulation, whereas monopolar stimulation had a broader activation than bipolar stimulation at the same depth. In more detail, the selectivity (depth/area) is shown in Figure 5B-1 and Figure 5-B2, which was consistently higher during bipolar stimulation than during monopolar stimulation at the same injection current. In addition, selectivity variation was marginal during monopolar stimulation for the different electrodes. In contrast, a smaller inter-electrode distance and larger electrode size increased selectivity in

bipolar stimulation. In both stimulations, an increment of the injection current reduced the selectivity.

3.3 Analysis of Other Factors Affecting Activation Maps

The effects of tumor thickness and conductivity, axon inclination, and resection border moisture on the activation maps are illustrated in Figure 6A–C. The effects were quantified based on the relative difference of the injection current between a model considering one of the three factors and the reference model (Figure 6D), as shown in Figure 6E and Figure 6F. The injection currents were required to achieve specific stimulation depths (1–5 mm) and areas (10–50 mm^2).

In both stimulations, the relative difference (depth and area) was lower than 30% for σ_{tumor} = 0.2 S/m, as shown in Figures 6-E1 and 6-F1. In contrast, the relative difference (depth and area) was higher than 30% for σ_{tumor} = 0.5 S/m for tumor thickness was larger than 2 mm during monopolar stimulation and 4 mm during bipolar stimulation. In general, the relative difference was smaller in bipolar stimulation than monopolar stimulation. No effects of the axon rotation were observed in the activation maps (Figure 6-E2 and Figure 6-F2). The relative differences were smaller than 5% in monopolar stimulation and 10% in bipolar stimulation. Figure 6-E3 and Figure 6-F3 show that dryer conditions decreased the injection current to achieve the same stimulation area and depth for both stimulations. Bipolar stimulation was more sensitive to moisture variations. The change in moisture thickness was more significant between 0.5 mm and 1 mm than that between 0.25 and 0.5 mm.

4. Discussion

Subcortical electrical stimulation is an intraoperative stimulation technique used during tumor resection to reduce the risk of CST injury (Shiban et al. 2015). Different stimulation parameters are used between different groups (Kamada et al. 2009; Saito et al. 2014; Fukaya et al. 2011; Raabe et al. 2014; Mikuni et al. 2007; Duffau et al. 2002; Ottenhausen et al. 2015). For the first

time, computational modeling of subcortical stimulation was implemented to improve the understanding of the interaction between neuronal elements and electrical stimulation. To achieve this, the effectiveness of our modeling was verified with experimental measurements of the threshold–distance relationship, as shown in Figure 3. A systematic sensitivity analysis of three parameters related to the stimulation was conducted, which are tumor, nerve inclination, and moisture.

4.1 Effect of Electrode Parameters on Stimulation

Figure 4 shows that the stimulation was dependent on electrode geometry in bipolar stimulation, whereas it was almost identical for various monopolar electrode geometries and reference electrode positions.

To quantify the stimulation region, the relationship between the activation depth and area was plotted, as shown in Figure 5. Regardless of the electrode configuration, we can achieve any point of the fitting curve if we change the injection current, but the lowest injection current is desirable. The lowest injection current to achieve the same point in the graph is possible by increasing the inter-electrode distance or decreasing the electrode diameter in bipolar stimulation. By increasing the inter-electrode distance, the stimulation approximates monopolar stimulation, in which the electrode diameter becomes less significant; however, a greater distance between the electrodes could make bipolar stimulation in confined regions more difficult. Experimental studies have also found that larger inter-electrode distances favor the elicitation of the pyramidal tract (Katayama et al. 1988). On the other hand, stimulation intensity did not vary between two different monopolar diameters (Szelényi et al. 2011) or the location of the reference electrode. Monopolar electrodes also require a lower injection current for activating the pyramidal cell's axon in the CST (Szelényi et al. 2011; Bello et al. 2014; Fukaya et al. 2011). The current with a bipolar electrode is more localized (Haglund et al. 1993), resulting in focal stimulation that may be useful for patients with a history of seizures.

4.2 Identification of CST Axons

Identification of the integrity of the motor pathway in the white matter during surgery is assessed based on the stimulation intensity that is correlated to the distance between the CST and the electrode (Kamada et al. 2009). Close to the resection border, the risk of a lesion increases, and the resolution of the stimulation intensity is important (Nossek et al. 2011). When comparing monopolar and bipolar stimulation (Figure 4), we observed that monopolar stimulation provided stronger activation for the same injection current. However, bipolar stimulation was more focal (i.e., greater penetration in a smaller area), as shown in Figure 5. For these reasons, monopolar stimulation can be useful to identify the CST at large distances from the resection border and a bipolar electrode at a short distance. In fact, a greater percentage of patients have positive responses (motor-evoked potentials (MEPs) or D-waves) to monopolar stimulation than to bipolar stimulation (90% vs. 50%) (Szelényi et al. 2011; Fukaya et al. 2011; Mikuni et al. 2007). However, the effectiveness of bipolar stimulation improves more for distances less than 1 cm (90% of responses) than for larger distances (20% of responses) (Mikuni et al. 2007). One study showed that the choice of the appropriate electrode depends on the clinical context and may change within the same surgery, according to ongoing modifications during the procedure (Bello et al. 2014). In our clinical experience, we have been able to detect MEPs in five of seven subjects if the stimulation point was located within 5 mm from the white matter bundle (confirmed by intraoperative diffusion-weighted imaging) using an electrode with 5 mm of inter-electrode distance and 3 mm in diameter (Ozawa et al. 2009). No responses were noted if the distance was greater than 5 mm, which agrees with the results in Figure 4B (right superior panel).

4.3 Analysis of Stimulation Factors

In Figure 6, we show that higher tumor conductivity or thickness affects the activation maps (smaller activation region). Their effects are limited as subcortical stimulation is mostly applied

at the end of resection procedure when most of the tumor has been resected. The effect of the axon orientation was also marginal (less than 5% and 10% for monopolar and bipolar stimulation, respectively).

Drier conditions can be affected by the CSF content change and irrigation fluids that are applied to the exposed brain to keep the brain surface and cavities moist and visible (Lewis & Elliott 1950; Kazim et al. 2010). Monopolar stimulation was less sensitive than bipolar stimulation to variations in moisture conditions (Figure 6). The reason for this is that the local current is shunted through the moisture between the electrodes in bipolar stimulation (Wongsarnpigoon & Grill 2008). Monopolar stimulation also did not change with possible variations in the electrode contact area, in contrast to bipolar stimulation—see Figure 4A. This finding can explain the results of one study in which the D-wave amplitude changed under bipolar stimulation (Fukaya et al. 2011). Accordingly, accumulation of any conductive substance, such as the CSF or blood, is drained, and the stimulated structure is kept dry in clinical practice. According to the previous discussion, the advantages of each stimulation type based on stimulation distance, selectivity, and robustness are summarized in Table 2.

4.4 Limitations

Our computational model has been verified in the stimulation threshold–distance relationship. There are three main factors affecting this relationship: axon thickness, uncertainty of tissue conductivity, and nerve modeling. The first factor is caused by the choice of axon thickness of the pyramidal cell's axons in the CST. The pyramidal tracts were assumed to be large-diameter axons (Betz's pyramidal cells) because they are activated first due to the inverse relationship between axon thickness and threshold, and MEPs are induced via direct excitation of Betz's pyramidal cells. The variability in the axon thickness has been reported to be between 10 and 15 μm on average (Rivara et al. 2003; Firmin et al. 2014; Guyton & Hall 2006). However, the statistics of axon thickness have not been reported until now, and thus, we applied a single axon thickness in our computation in the reported range. In the second factor, a single tissue (white

matter) is essential to characterize the activation of the CST in our volume conductor modeling, and its uncertainty is not sufficiently high, as reported previously (C. Gabriel et al. 1996). Anisotropic characteristics of the white matter tissue were also not considered; however, activation maps with less depth are expected. The last factor affecting the relationship is the nerve model used to investigate the effect of stimulation parameters for subcortical stimulation. Despite these simplifications, the implemented subcortical model is reasonable in the regime considered here and similar general methodology applied here can be used to other white matter tracts (e.g., arcuate fasciculus when operating on regions close to Broca's and Wernicke's areas).

5. Conclusions

This study investigated the influence of different electrode geometries in monopolar and bipolar stimulation used by different clinical groups. For the first time, verified computational modeling of subcortical stimulation was implemented to clarify the interaction between neuronal elements and electrical stimulation in the subcortical region to characterize the stimulation parameters. The stimulation occurred in the vicinity of the cathodic electrode in bipolar stimulation. Monopolar stimulation had a broader activation region than bipolar stimulation for the same injection current. If the CST is close to the resection border, bipolar stimulation can produce more selective activation with more sensitivity than monopolar stimulation. However, monopolar stimulation is more robust to variations in the electrode contact area and moisture conditions, as well as being more effective for the CST far from the stimulation point.

Declarations of interest: none

Acknowledgments

This study was supported by a JSPS Grant-in-Aid for Scientific Research, JSPS KAKENHI Grant-17H05293 and 17H05306.

References

Aonuma, S. et al., 2018. A high-resolution computational localization method for transcranial magnetic stimulation mapping. *NeuroImage*, 172, pp.85–93.

Bello, L. et al., 2014. Tailoring neurophysiological strategies with clinical context enhances resection and safety and expands indications in gliomas involving motor pathways. *Neuro-oncology*, 16(8), pp.1110–28.

Christidi, F. et al., 2016. Fiber tracking: A qualitative and quantitative comparison between four different software tools on the reconstruction of major white matter tracts. *European journal of radiology open*, 3, pp.153–61.

Dale, A.M., Fischl, B. & Sereno, M.I., 1999. Cortical Surface-Based Analysis. *NeuroImage*, 9(2), pp.179–194.

Dawson, T.W. & Stuchly, M.A., 1998. High-resolution organ dosimetry for human exposure to low-frequency magnetic fields. *IEEE Transactions on Magnetics*, 34(3), pp.708–718.

Deng, Z.-D., Lisanby, S.H. & Peterchev, A. V., 2013. Electric field depth–focality tradeoff in transcranial magnetic stimulation: Simulation comparison of 50 coil designs. *Brain Stimulation*, 6(1), pp.1–13.

Duffau, H. et al., 2002. Intraoperative mapping of the subcortical language pathways using direct stimulations. An anatomo-functional study. *Brain : a journal of neurology*, 125(Pt 1), pp.199–214.

Enatsu, R. et al., 2016. Intraoperative Subcortical Fiber Mapping with Subcortico-Cortical Evoked Potentials. *World Neurosurgery*, 86, pp.478–483.

Firmin, L. et al., 2014. Axon diameters and conduction velocities in the macaque pyramidal tract. *Journal of Neurophysiology*, 112(6).

Fukaya, C. et al., 2011. Corticospinal descending direct wave elicited by subcortical stimulation. *Journal of Clinical*, 28(3), pp.297–301.

Gabriel, C., Gabriel, S. & Corthout, E., 1996. The dielectric properties of biological tissues: I. Literature survey. *Physics in medicine and biology*, 41(11), p.2231.

Gabriel, S., Lau, R.W. & Gabriel, C., 1996. The dielectric properties of biological tissues: III. Parametric models for the dielectric spectrum of tissues. *Physics in Medicine and Biology*, 41(11), pp.2271–2293.

Gomez-Tames, J., Hamasaka, A., et al., 2018. Atlas of optimal coil orientation and position for TMS: A computational study. *Brain Stimulation*, 11(4), pp.839–848.

Gomez-Tames, J., Akimasa, H., et al., 2018. Corticomotoneuronal Model for Intraoperative Neurophysiological Monitoring During Direct Brain Stimulation. *International Journal of Neural Systems*.

Gomez-Tames, J., Gonzalez, J. & Yu, W., 2012. A simulation study: Effect of the inter-electrode distance, electrode size and shape in Transcutaneous Electrical Stimulation. In *Engineering in Medicine and Biology Society (EMBC)*. San Diego: Annual International Conference of the IEEE, pp. 3576–3579.

Gomez-Tames, J., Gonzalez, J. & Yu, W., 2013. A Simulation Study on the Dominance of the Tissues' Conductivity in the Muscle Recruitment. *Journal of Medical Imaging and Health Informatics*, 3(1), pp.72–78.

Guyton, A.C. & Hall, J.E. (John E., 2006. *Textbook of medical physiology*, Elsevier Saunders.

Haglund, M.M., Ojemann, G.A. & Blasdel, G.G., 1993. Optical imaging of bipolar cortical stimulation. *Journal of Neurosurgery*, 78(5), pp.785–793.

Hervey-Jumper, S.L. et al., 2015. Awake craniotomy to maximize glioma resection: methods and technical nuances over a 27-year period. *Journal of Neurosurgery*, 123(2), pp.325–339.

Iwahashi, M. et al., 2017. Evaluation method for *in situ* electric field in standardized human brain for different transcranial magnetic stimulation coils. *Physics in Medicine and Biology*, 62(6), pp.2224–2238.

Janssen, A.M., Oostendorp, T.F. & Stegeman, D.F., 2014. The effect of local anatomy on the electric field induced by TMS: evaluation at 14 different target sites. *Medical & Biological Engineering & Computing*, 52(10), pp.873–883.

Kamada, K. et al., 2009. The motor-evoked potential threshold evaluated by tractography and electrical stimulation. *Journal of neurosurgery*, 111(4), pp.785–95.

Katayama, Y. et al., 1988. Corticospinal direct response in humans: identification of the motor cortex during intracranial surgery under general anaesthesia. *Journal of neurology, neurosurgery, and psychiatry*, 51(1), pp.50–9.

Kazim, S.F., Enam, S.A. & Shamim, M.S., 2010. Possible detrimental effects of neurosurgical irrigation fluids on neural tissue: An evidence based analysis of various irrigants used in contemporary neurosurgical practice. *International Journal of Surgery*, 8(8), pp.586–590.

Laakso, I. et al., 2015. Inter-subject Variability in Electric Fields of Motor Cortical tDCS. *Brain Stimulation*, 8(5), pp.906–913.

Laakso, I. & Hirata, A., 2012. Fast multigrid-based computation of the induced electric field for transcranial magnetic stimulation. *Physics in medicine and biology*, 57(23), pp.7753–7765.

Laakso, I., Hirata, A. & Ugawa, Y., 2014. Effects of coil orientation on the electric field induced by TMS over the hand motor area. *Physics in Medicine and Biology*, 59(1), pp.203–218.

Latikka, J., Kuurne, T. & Eskola, H., 2001. Conductivity of living intracranial tissues. *Physics in medicine and biology*, 46(6), pp.1611–6.

Lewis, R.C. & Elliott, K.A.C., 1950. Clinical Uses of an Artificial Cerebrospinal Fluid. *Journal of Neurosurgery*, 7(3), pp.256–260.

Lu, Y. et al., 1992. Dielectric properties of human glioma and surrounding tissue. *International journal of hyperthermia*, 8(6), pp.755–60.

Mandonnet, E. & Pantz, O., 2011. The role of electrode direction during axonal bipolar electrical stimulation: a bidomain computational model study. *Acta Neurochirurgica*, 153(12), pp.2351–2355.

Manola, L. et al., 2005. Modelling motor cortex stimulation for chronic pain control: electrical potential field, activating functions and responses of simple nerve fibre models. *Medical & biological engineering & computing*, 43(3), pp.335–43.

McNeal, D., 1976. Analysis of a model for excitation of myelinated nerve. *IEEE Transactions on Biomedical Engineering*, 4, pp.329–337.

Mikuni, N. et al., 2007. Clinical impact of integrated functional neuronavigation and subcortical electrical stimulation to preserve motor function during resection of brain tumors. *Journal of Neurosurgery*, 106(4), pp.593–598.

Nossek, E. et al., 2011. Intraoperative mapping and monitoring of the corticospinal tracts with neurophysiological assessment and 3-dimensional ultrasonography-based navigation. *Journal of neurosurgery*, 114(3), pp.738–46.

Nummenmaa, A. et al., 2014. Targeting of White Matter Tracts with Transcranial Magnetic Stimulation. *Brain Stimulation*, 7(1), pp.80–84.

Ottenhausen, M. et al., 2015. Functional preoperative and intraoperative mapping and monitoring: increasing safety and efficacy in glioma surgery. *Neurosurgical Focus*, 38(1), p.E3.

Ozawa, N. et al., 2009. Identification of the Pyramidal Tract by Neuronavigation Based on Intraoperative Diffusion-Weighted Imaging Combined with Subcortical Stimulation. *Stereotactic and Functional Neurosurgery*, 87(1), pp.18–24.

Prabhu, S.S. et al., 2011. Intraoperative magnetic resonance imaging–guided tractography with integrated monopolar subcortical functional mapping for resection of brain tumors. *Journal of Neurosurgery*, 114(3), pp.719–726.

Raabe, A. et al., 2014. Continuous dynamic mapping of the corticospinal tract during surgery of motor eloquent brain tumors: evaluation of a new method. *Journal of Neurosurgery*, 120(5), pp.1015–1024.

Rattay, F., 1999. The basic mechanism for the electrical stimulation of the nervous system. *Neuroscience*, 89(2), pp.335–346.

Riva, M. et al., 2016. Monopolar high-frequency language mapping: can it help in the surgical management of gliomas? A comparative clinical study. *Journal of neurosurgery*, 124(5), pp.1479–89.

Rivara, C. et al., 2003. Stereologic characterization and spatial distribution patterns of Betz cells in the human primary motor cortex. *The Anatomical Record*, 270A(2), pp.137–151.

Saito, T. et al., 2014. Intraoperative cortico-cortical evoked potentials for the evaluation of language function during brain tumor resection: initial experience with 13 cases. *Journal of Neurosurgery*, 121(4), pp.827–838.

Saito, T. et al., 2015. Intraoperative functional mapping and monitoring during glioma surgery. *Neurologia medico-chirurgica*, 55(1), pp.1–13.

Seo, H. et al., 2017. A multi-scale computational model of the effects of TMS on motor cortex. *F1000Research*, 5, p.1945.

Seo, H., Kim, D. & Jun, S.C., 2015. Computational Study of Subdural Cortical Stimulation: Effects of Simulating Anisotropic Conductivity on Activation of Cortical Neurons. *PloS one*, 10(6), p.e0128590.

Shiban, E. et al., 2015. Intraoperative subcortical motor evoked potential stimulation: how close is the corticospinal tract? *Journal of Neurosurgery*, 123(3), pp.711–720.

Smith, J.S. et al., 2008. Role of Extent of Resection in the Long-Term Outcome of Low-Grade Hemispheric Gliomas. *Journal of Clinical Oncology*, 26(8), pp.1338–1345.

Song, B. et al., 2016. Numeric Investigation of Brain Tumor Influence on the Current Distributions During Transcranial Direct Current Stimulation. *IEEE Transactions on Biomedical Engineering*, 63(1), pp.176–187.

Sweeney, J.D., Mortimer, J.T. & Durand, D., 1987. Modeling of mammalian myelinated nerve for functional neuromuscular electrostimulation. *IEEE 97th Annual Conf. Engineering in Medicine Biology Society, Boston*, 9, pp.1577–1578.

Szelényi, A. et al., 2011. Intra-operative subcortical electrical stimulation: a comparison of two methods. *Clin Neurophysiol*, 122(7), pp.1470–1475.

Szelényi, A. et al., 2010. Intraoperative electrical stimulation in awake craniotomy: methodological aspects of current practice. *Neurosurgical focus*, 28(2), p.E7.

Voigt, T. et al., 2011. In vivo glioma characterization using MR conductivity imaging. *Proceedings of the 19th Scientific Meeting of the International Society of Magnetic Resonance in Medicine*, 127.

Wongsarnpigoon, A. & Grill, W.M., 2008. Computational modeling of epidural cortical stimulation. *Journal of neural engineering*, 5(4), pp.443–54.

Yamaguchi, F., Takahashi, H. & Teramoto, A., 2007. Intra-operative detection of motor pathways using a simple electrode provides safe brain tumor surgery. *Journal of Clinical Neuroscience*, 14(11), pp.1106–1110.

Figures and Tables

Figure 1. Subcortical Stimulation Model. (A) Realistic head model with a craniotomy. A coronal cut reveals most of the internal tissues in the head model. Positions of the cathodic and anodic electrodes are also indicated. Note that only one anode is used at the same time. Representative voltage distributions using an injection current of 15 mA for (B) monopolar with the distant anodic electrode (reference electrode) on the left side of the neck and (C) bipolar stimulation.

Figure 2. Activation Map. (A) The CST axons are placed in a grid near the cathodic electrode. The CST axons correspond to the CRRSS model to compute the action potential at the threshold injected current. Note that the CST axons run along the superior–inferior direction. (B) The activation map corresponds to the distribution of the threshold current in the grid plane. For illustration, two indices used in this study (stimulation area and depth) are depicted for an injection current of 15 mA. CST, corticospinal tract; CRRSS, Chiu–Ritchie–Rogart–Stagg–Sweeney.

Figure 3. Direct subcortical electrical stimulation model verification. Computation of the stimulation intensity of direct axon stimulation at different distances from the resection border agrees with experimental results presented in (Kamada et al. 2009). Axon diameters are selected between 11 μm and 15 μm.

Figure 4. Activation maps for different electrode geometries using monopolar and bipolar stimulation.

Figure 5. Relationship between stimulation depth and area at four stimulation currents for (A1) monopolar and (A2) bipolar stimulation. Note that the different electrode diameters overlap for

the same injection current in monopolar stimulation. (B1–B2) Selectivity (depth/area) of monopolar and bipolar stimulation.

Figure 6. Analysis of possible factors affecting the activation maps. (A) Tumor thickness and conductivity, (B) axon inclination, and (C) moisture thickness. (D) Activation maps with reference conditions ($\sigma_{tumor} = \sigma_{white\text{-}matter}$, moisture thickness = 0.5 mm, axon inclination = 0 [deg]). (E and F) Variability in the injection current due to the factors (A–C) with respect to the reference map (D). The injection currents are set to achieve 1–5 mm of stimulation depth and 10–50 mm^2 of stimulation area.

Table 1. Stimulation conditions

Table 2. Selection criteria

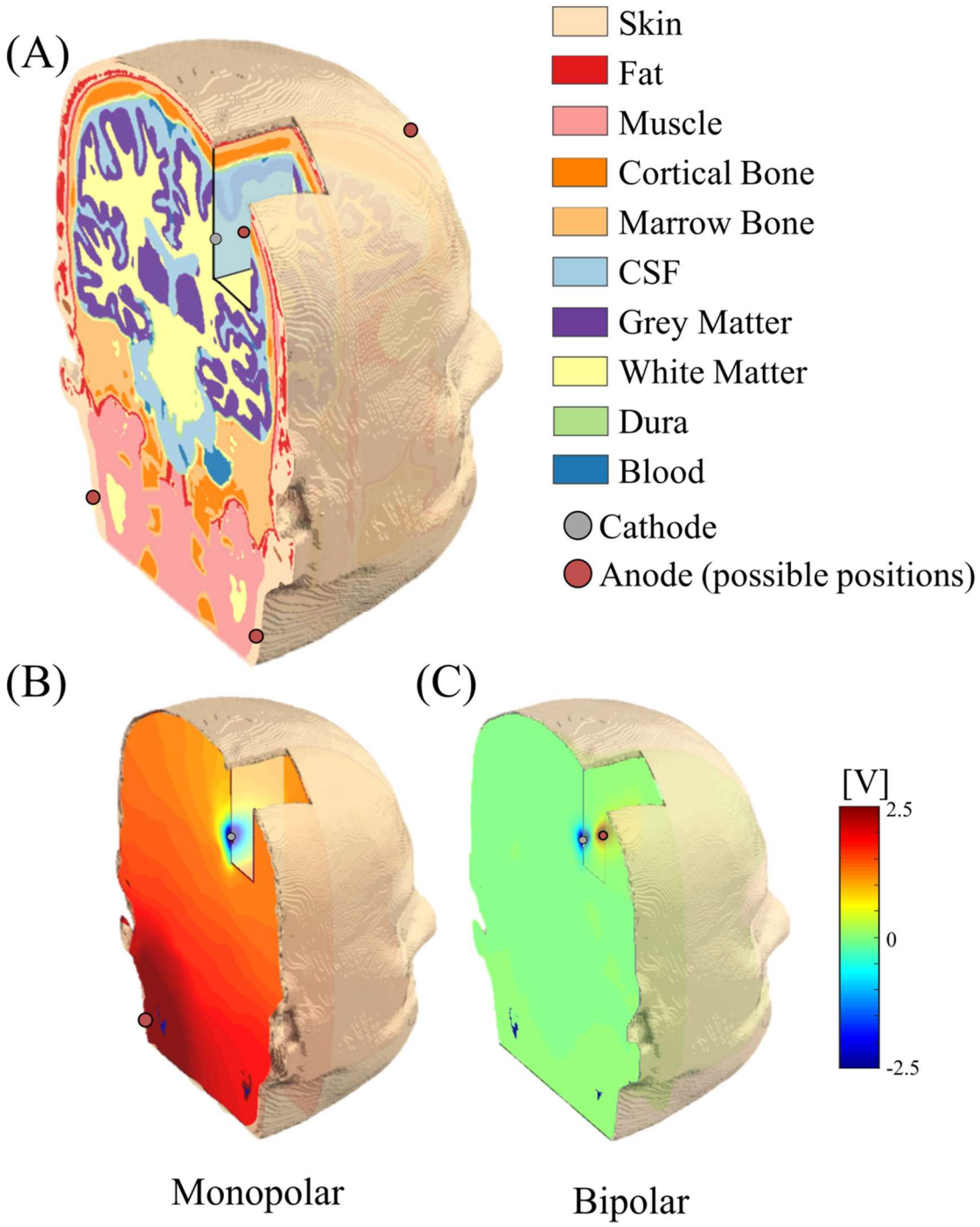
(A)
Skin
Fat
Muscle
Cortical Bone
Marrow Bone
CSF
Grey Matter
White Matter
Dura
Blood
Cathode
Anode (possible positions)
(B)
(C)
[V]
2.5
0
-2.5
Monopolar
Bipolar

Figure 1

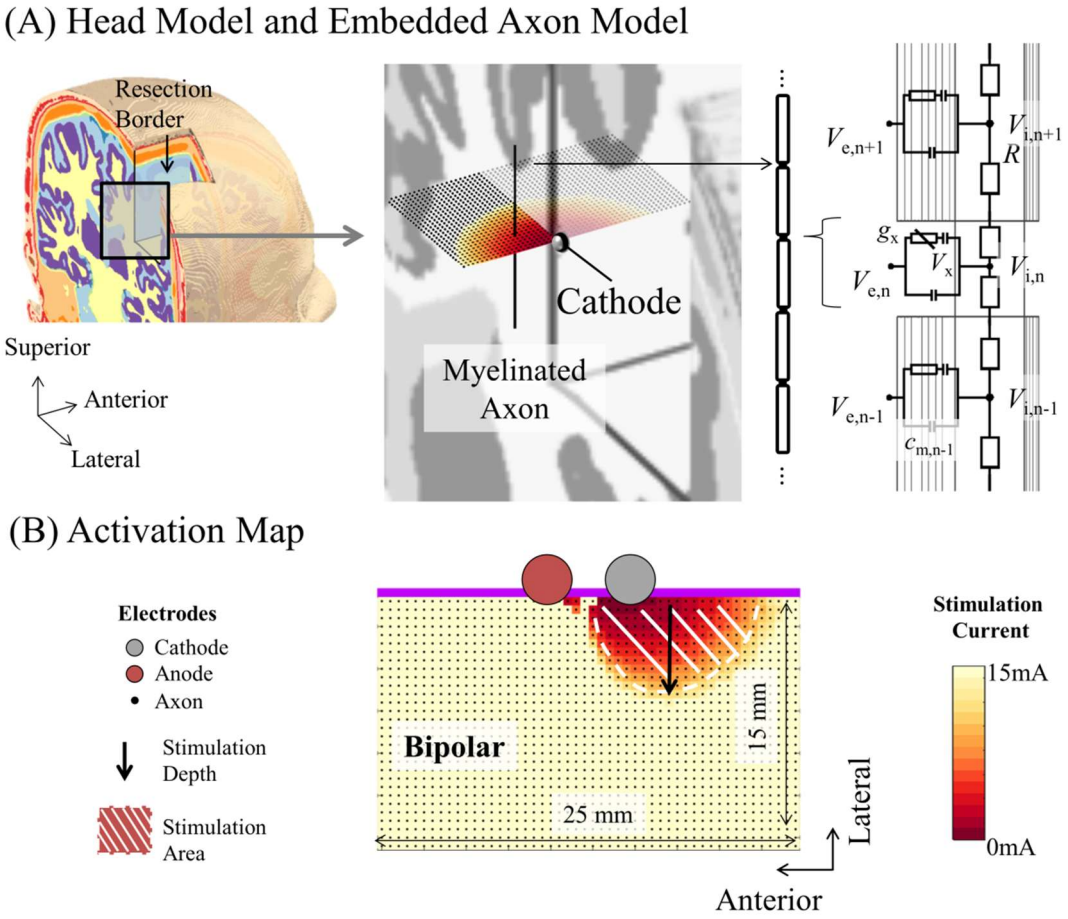
(A) Head Model and Embedded Axon Model
Resection Border
Superior
Anterior
Lateral
Cathode
Myelinated Axon
$V_{e,n+1}$
$V_{i,n+1}$
R
g_x
V_x
$V_{e,n}$
$V_{i,n}$
$V_{e,n-1}$
$V_{i,n-1}$
$c_{m,n-1}$
(B) Activation Map
Electrodes
Cathode
Anode
Axon
Stimulation Depth
Stimulation Area
Bipolar
15 mm
25 mm
Lateral
Anterior
Stimulation Current
15mA
0mA

Figure 2

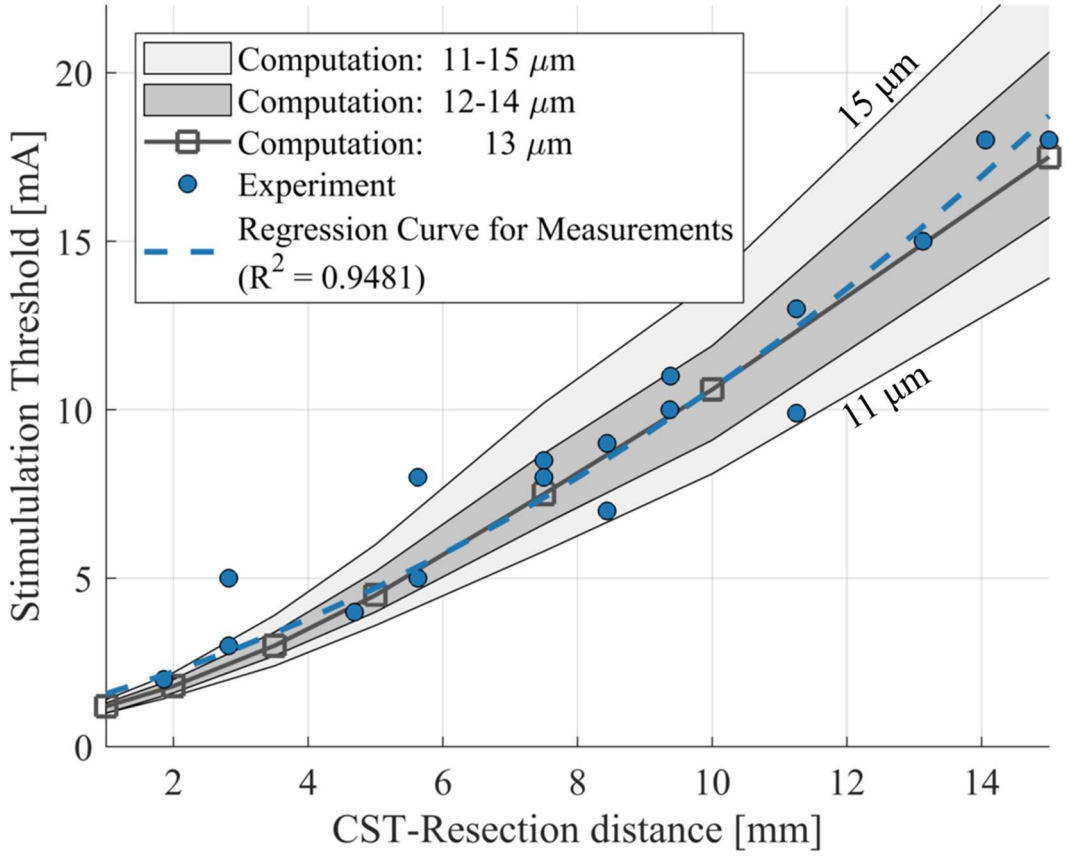
Computation: 11-15 μm
Computation: 12-14 μm
Computation: 13 μm
Experiment
Regression Curve for Measurements
(R2 = 0.9481)
15 μm
11 μm
Stimulation Threshold [mA]
CST-Resection distance [mm]
0
5
10
15
20
2
4
6
8
10
12
14

Figure 3

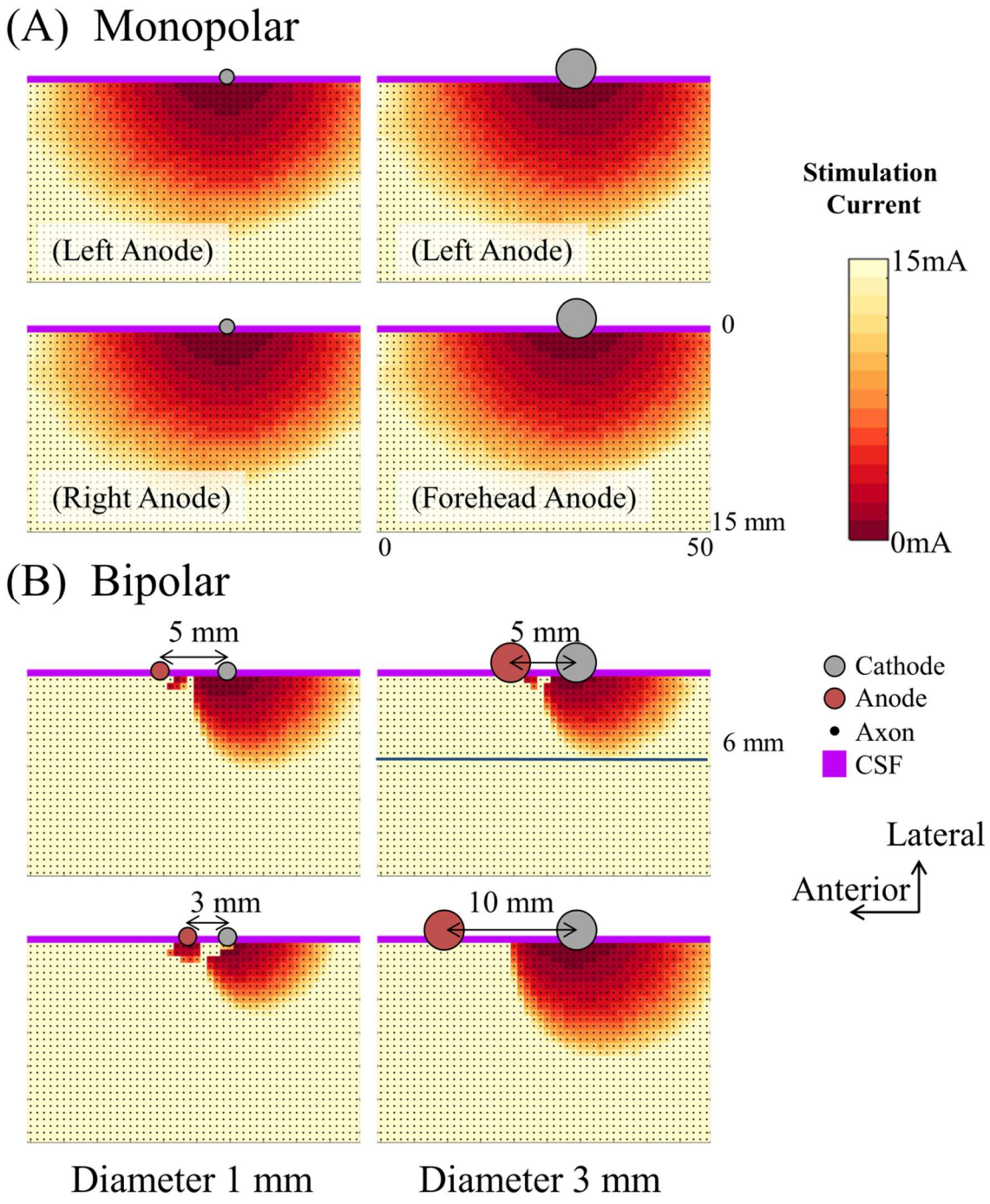
(A) Monopolar
(Left Anode)
(Left Anode)
(Right Anode)
(Forehead Anode)
0
15 mm
0
50
Stimulation Current
15mA
0mA
(B) Bipolar
5 mm
5 mm
6 mm
3 mm
10 mm
Cathode
Anode
Axon
CSF
Lateral
Anterior
Diameter 1 mm
Diameter 3 mm

Figure 4

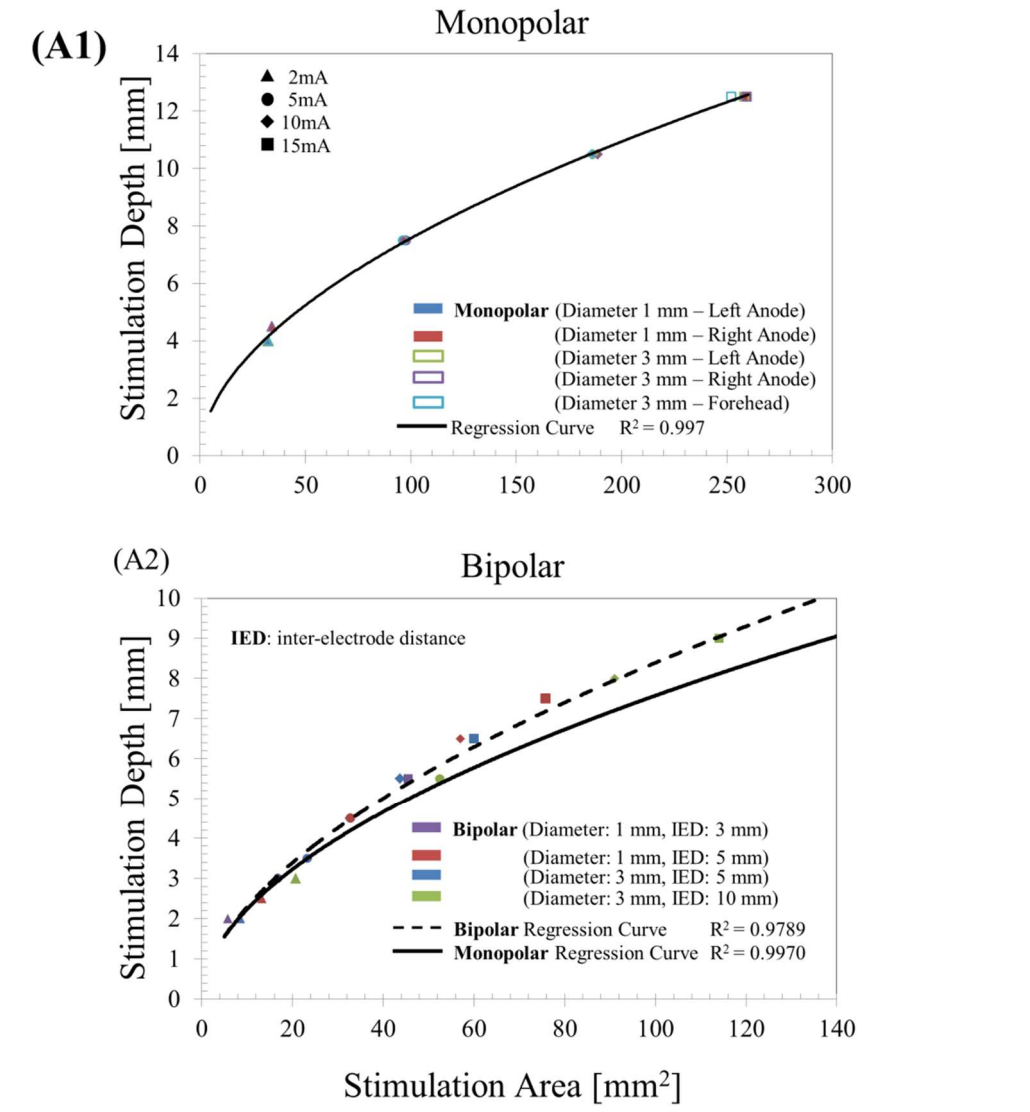
(A1)
Monopolar
Stimulation Depth [mm]
2mA
5mA
10mA
15mA
Monopolar (Diameter 1 mm – Left Anode)
(Diameter 1 mm – Right Anode)
(Diameter 3 mm – Left Anode)
(Diameter 3 mm – Right Anode)
(Diameter 3 mm – Forehead)
Regression Curve R² = 0.997
(A2)
Bipolar
IED: inter-electrode distance
Stimulation Depth [mm]
Bipolar (Diameter: 1 mm, IED: 3 mm)
(Diameter: 1 mm, IED: 5 mm)
(Diameter: 3 mm, IED: 5 mm)
(Diameter: 3 mm, IED: 10 mm)
Bipolar Regression Curve R² = 0.9789
Monopolar Regression Curve R² = 0.9970
Stimulation Area [mm²]
(B1)
(B2)
Selectivity
Diameter 1 mm
Diameter 3 mm
Left
Right
Left
Forehead
Right
Anode Position
2 mA
5 mA
10 mA
15 mA
3
5
5
10
Inter-electrode distance (mm)

Figure 5

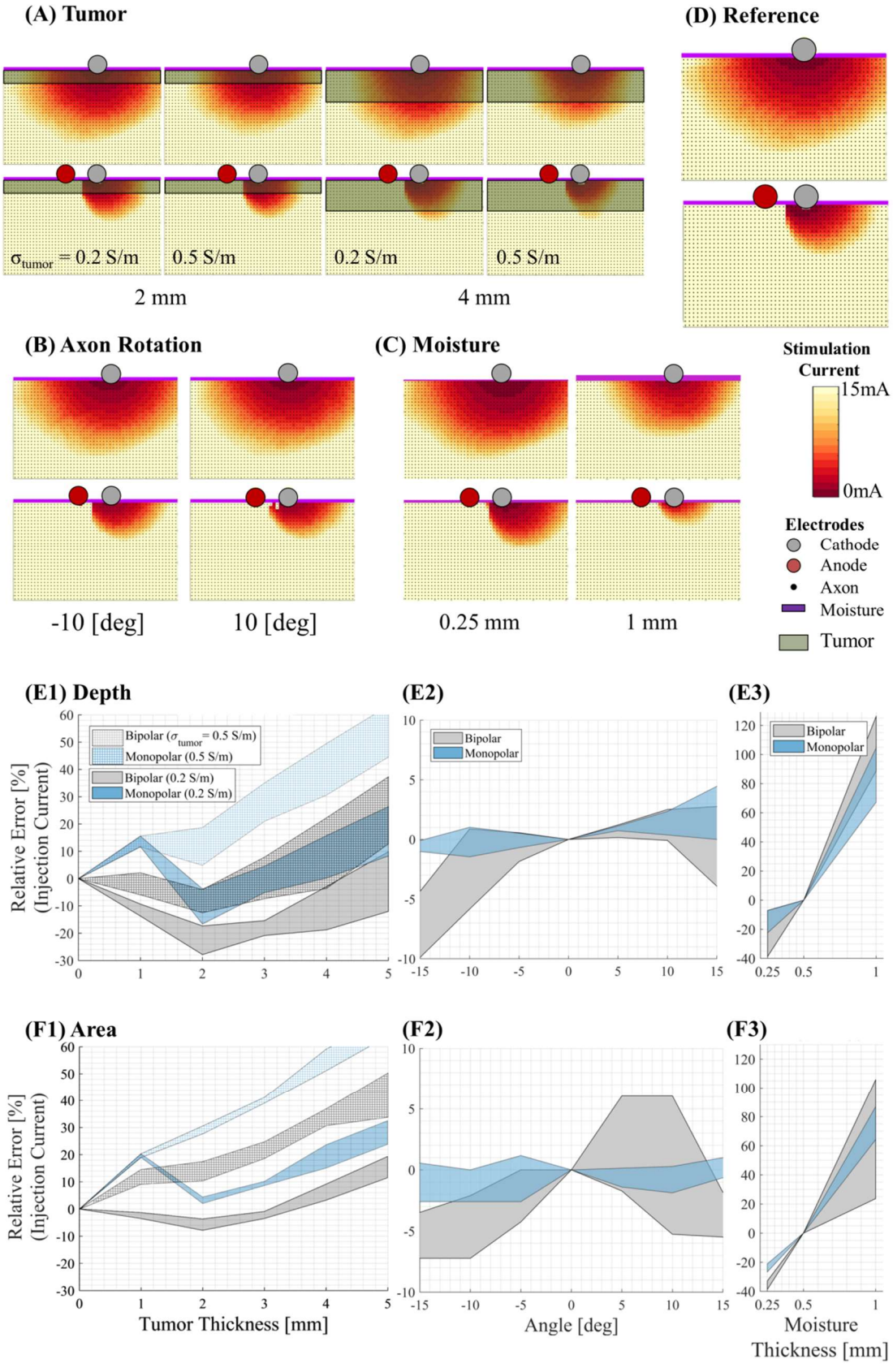
(A) Tumor
(D) Reference
σtumor = 0.2 S/m
0.5 S/m
0.2 S/m
0.5 S/m
2 mm
4 mm
(B) Axon Rotation
(C) Moisture
Stimulation Current
15mA
0mA
Electrodes
Cathode
Anode
Axon
Moisture
Tumor
-10 [deg]
10 [deg]
0.25 mm
1 mm
(E1) Depth
(E2)
(E3)
Bipolar (σtumor = 0.5 S/m)
Monopolar (0.5 S/m)
Bipolar (0.2 S/m)
Monopolar (0.2 S/m)
Bipolar
Monopolar
Relative Error [%] (Injection Current)
(F1) Area
(F2)
(F3)
Tumor Thickness [mm]
Angle [deg]
Moisture Thickness [mm]

Figure 6

Table 1

Configuration	Electrode Diameter	Inter-electrode Distance	Ground Electrode
Monopolar	1 or 3 mm	N.A.	Left/right below ear or forehead
Bipolar	1 mm	3 or 5 mm	N.A.
	3 mm	5 or 10 mm	

Table 2

Criteria	Recommendation
Short Distance (<5 mm)	Bipolar
Selectivity	Bipolar
Long Distance (>5 mm)	Monopolar
Robustness	Monopolar*

* Moisture and contact electrode area